Computational Assessment and Understanding of C₆ Product Selectivity for Chromium Phosphinoamidine Catalyzed Ethylene Trimerization

Nathan Morgan,[1] Steven M. Maley,[1] Doo-Hyun Kwon,[1] Michael S. Webster-Gardiner,[2] Brooke L. Small,[2] Orson. L. Sydora,[2] Steven. M. Bischof,[2]* and Daniel H. Ess[1]*
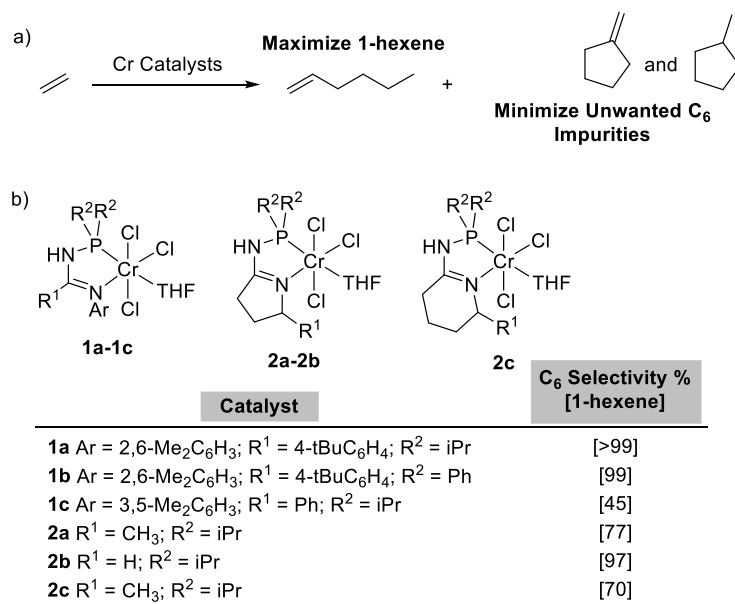
[1]Department of Chemistry and Biochemistry, Brigham Young University, Provo, Utah 84602 (USA). [2]Research and Technology, Chevron Phillips Chemical Company LP, 1862 Kingwood Drive, Kingwood, Texas 77339 (USA)

Abstract

One approach to selectively generate 1-hexene is through ethylene trimerization using highly active Cr *N*-phosphinoamidine catalysts ((P,N)Cr). Depending on the ligand, (P,N)Cr catalysts can either generate nearly pure 1-hexene or form 1-hexene with significant mixtures of other C_6 mass products, for example methylenecyclopentane. Here we report DFT transition state modeling examining 1-hexene catalysis pathways as well as pathways that lead to alternative C_6 mass products. This provided qualitative and semi-quantitative modeling of the experimental 1-hexene purity values for several (P,N)Cr catalysts. Consistent with previous computational studies, the key 1-hexene purity-determining transition states were determined to be *β*-hydrogen transfer structures from the metallacycloheptane intermediate. The origin of selectivity for these (P,N)Cr catalysts can be attributed to steric effects in the transition-state structure with coordinated ethylene that leads to C_6 impurities.

Introduction

1-Hexene is a key component in the manufacturing of high-performance polyethylene (PE). This plastic resin is commonly used in the production of film and rigid containers for a variety of everyday products, including packaging for food, detergent and pharmaceuticals, among many others.[1,2] One approach to the selective generation of 1-hexene is ethylene trimerization using Cr-phosphine molecular catalysts (Scheme 1a).[3,4,5,6] Effective catalysis requires fast reactivity as well as selectivity that maximizes 1-hexene and minimizes all other oligomerization products, especially other C_6 mass products (e.g. methylenecyclopentane). We previously used density functional theory (DFT) calculations to understand why Cr *N*-phosphinoamidine catalysts ((P,N)Cr) provide high reactivity for ethylene trimerization.[7] We also previously used DFT calculations to predict 1-hexene versus 1-octene linear α-olefin selectivity.[8] We have not reported calculations evaluating selectivity of 1-hexene versus alternative C_6 mass products (also called 1-hexene purity) for (P,N)Cr catalysts.

| Catalyst	C_6 Selectivity % [1-hexene]
1a Ar = 2,6-Me$_2$C$_6$H$_3$; R^1 = 4-tBuC$_6$H$_4$; R^2 = iPr	[>99]
1b Ar = 2,6-Me$_2$C$_6$H$_3$; R^1 = 4-tBuC$_6$H$_4$; R^2 = Ph	[99]
1c Ar = 3,5-Me$_2$C$_6$H$_3$; R^1 = Ph; R^2 = iPr	[45]
2a R^1 = CH$_3$; R^2 = iPr	[77]
2b R^1 = H; R^2 = iPr	[97]
2c R^1 = CH$_3$; R^2 = iPr	[70]

Scheme 1. a) Example of Cr catalyzed ethylene trimerization to 1-hexene. b) Previously reported Chevron Phillips Chemical Co. LP (P,N)Cr catalysts for ethylene trimerization.

Depending on the ligand, (P,N)Cr catalysts can range from generating nearly pure 1-hexene to forming a nearly equal mixture of 1-hexene versus other C_6 products. Sydora and coworkers previously reported aryl and benzyl *N*-phosphinoamidine (P,N)Cr catalysts with a wide range of C_6 selectivity.[9] For example, catalyst **1a** with a 2,6-dimethyl aryl substituted imine and an isopropyl phosphine gave 94% mass selectivity for C_6 products with >99% 1-hexene selectivity versus all other C_6 products (Scheme 1b). In contrast, the similar catalyst **1c** with the major difference compared to **1a** being a 3,5-dimethyl aryl substituted imine ligand gave less than 50% 1-hexene. For our new monocyclic imine ligand catalysts, **2a-2c**, there is a 70-97% range in 1-hexene selectivity for C_6 products.[10]

Because there are no simple empirical based rules to predict 1-hexene purity, and previous computational studies only evaluated one major bisphosphine Cr catalyst system without quantitative comparison to experiment,[11] we executed calculations to determine if the (P,N)Cr experimental values could be qualitatively or quantitatively modeled with DFT transition states, which can then enable more detailed computational design and evaluation of possible 1-hexene catalysts. By calculating many reasonable pathways that branch from the 1-hexene catalytic cycle, we found that DFT transition states combined with transition-state theory provides qualitative and semi-quantitative replication of experimental 1-hexene purity values. This also revealed the key purity-determining transition states. These transition states revealed that the 2,6-dimethyl aryl ligand of catalyst **1a**, compared to the 3,5-dimethyl aryl ligand of catalyst **1c**, sterically intrudes into the Cr coordination sphere to create very high 1-hexene selectivity by altering the relative energy of the metallacycloheptane to *β*-hydrogen transfer reaction step.

Results and Discussion

1-Hexene catalytic mechanism and mechanisms to give alternative C₆ products. The lowest energy catalytic cycle for 1-hexene formation by (P,N)Cr catalysts is outlined with black arrows in Scheme 2. We previously used this catalytic cycle to predict 1-hexene/1-octene selectivity and design new catalysts that were experimentally realized.[8] This chromacycle mechanism was proposed by Manyik more than 40 years ago,[12,13] and DFT calculations by Britovsek and McGuinness,[11,14,15] Cheong,[16] Liu,[17] and others[18,19,20,21,22] have also proposed similar catalytic mechanisms for ethylene oligomerization for related Sasol and Phillips type systems. The 1-hexene mechanism has also been computationally evaluated under H_2 conditions.[23,24] Importantly, this catalytic cycle is consistent with several experimental studies,[25,26,27,28,29] including deuterium labeling experiments.[4,5,30,31,32,33]
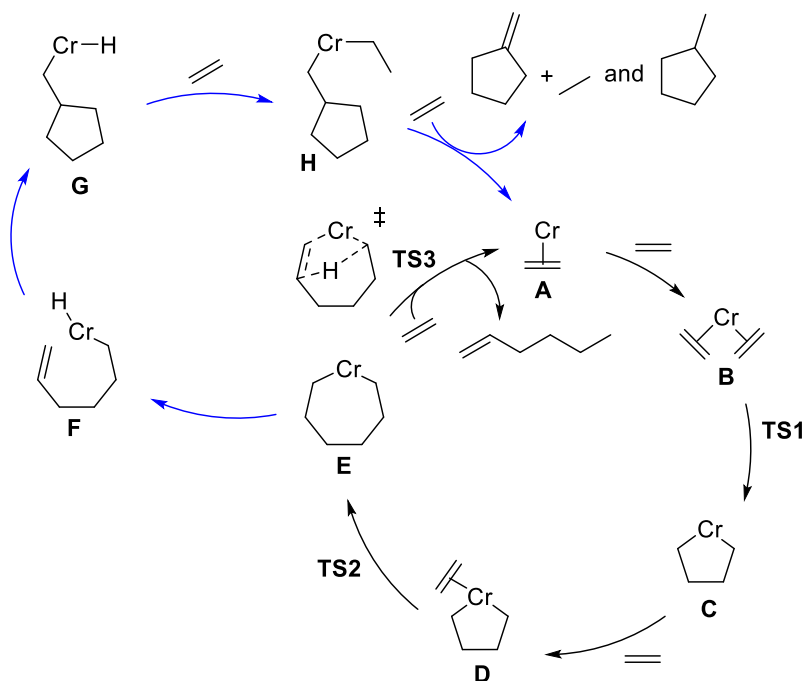
Scheme 2. The black arrows outline the lowest energy catalytic cycle for (P,N)Cr-catalyzed ethylene trimerization to 1-hexene. The blue arrows outline one possible alterative C₆ pathway to methylenecyclopentane and ethane.

The 1-hexene catalytic cycles begins with a (mono)ethylene Cr-species **A** followed by ethylene coordination and oxidative C-C bond coupling to give chromacyclopentane **C**. A third ethylene coordination gives intermediate **D** and migratory insertion leads to the chromacycloheptane intermediate **E** that can produce 1-hexene via β-hydrogen transfer (βHT). Similar to Britovsek and McGuinness,[11,14,15] we have used a $Cr^{I/III}$ cycle with spin crossover (sextet to quartet) rather than a $Cr^{II/IV}$ cycle. However, older calculations, typically with model ligands (e.g. chlorides), suggested a metallacycle $Cr^{II/IV}$ cycle.[34] While there are several possible branches from this 1-hexene catalytic cycle to make alternative C_6 products, one pathway to methylenecyclopentane is outlined with blue arrows in Scheme 2. This methylenecyclopentane forming pathway involves chromacycloheptane intermediate **E** that undergoes β-hydrogen elimination to give the Cr-H **F** followed by two sequential migratory insertion steps to give the (cyclopentylmethyl)Cr(ethyl) intermediate **H**. This intermediate can undergo β-hydrogen elimination to give methylenecyclopentane and ethane. Alternatively, this intermediate can generate methylcyclopentane and ethylene.

Scheme 3 outlines several pathways that branch from intermediate **E** to give alternative C_6 products. For example, direct reductive elimination from **E** gives cyclohexane. Intermediates **F**, **G**, and **H** were described in the alternative catalytic cycle in Scheme 2. It is also possible for secondary branches to lead to alternative C_6 products. For example, from the (cyclopentylmethyl)Cr(H) intermediate **G**, reductive elimination leads to methylcyclopentane. Also, ethylene coordination to **G** followed by β-hydrogen transfer also gives methylcyclopentane. There is also the possibility of structures **F** and **G** being circumvented by first ethylene coordination to **E** to give **I** followed β-hydrogen transfer and migratory insertion to give **H**. While not considered here, it is important to point out that there is also the possibility for alternative

higher mass products to be generated from intermediates in the Scheme 2 cycle. For example, C_{10} products (e.g. decenes) can be formed if oligomerization incorporates two ethylenes and one 1-hexene.[35]
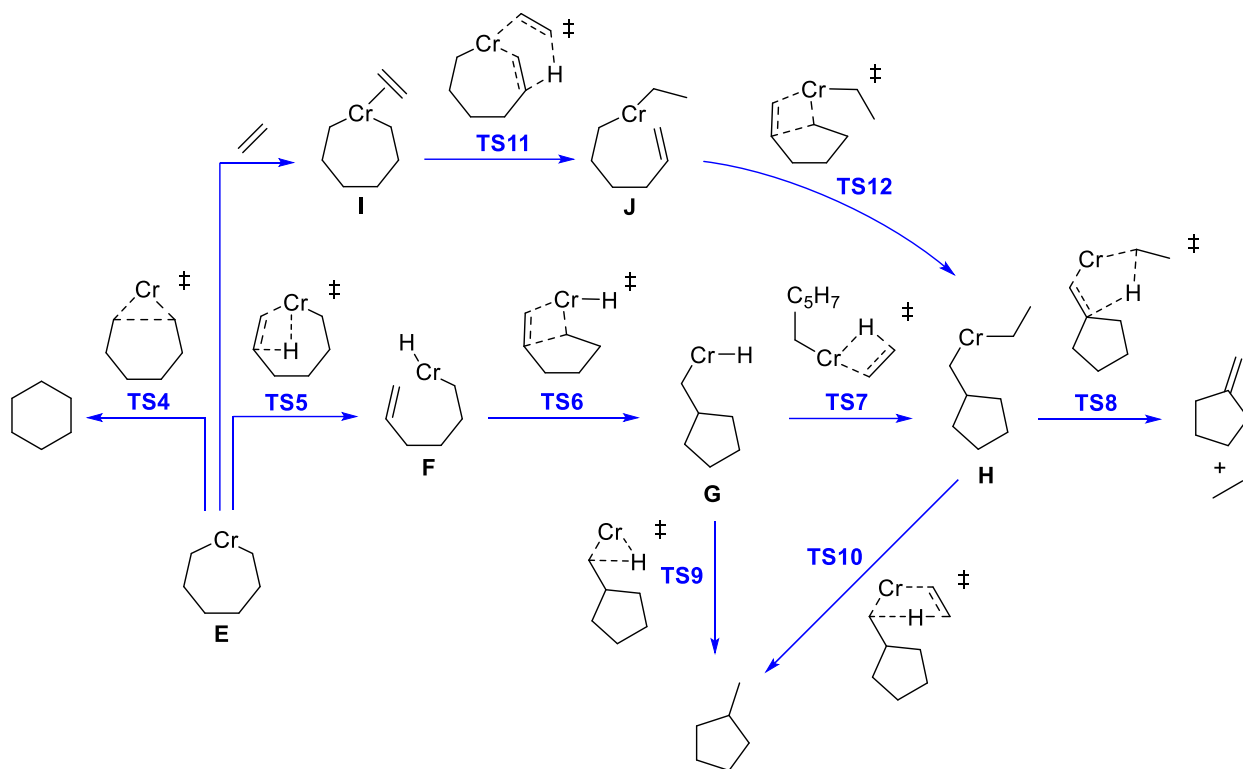
Scheme 3. Outline of pathways from intermediate **E** to alterative (non-1-hexene) C_6 mass products.

Computational details. Because our previous DFT calculations showed very high correlation with experimental values for 1-hexene/1-octene selectivity, we used the same general computational methodology here for 1-hexene purity.[8] The use of the M06-L[36] density functional was motived by the work of McGuinness and Britovsek who showed that this functional gave similar spin-state and reaction energies compared to accurate wavefunction methods.[37] The unrestricted M06-L functional with an ultrafine integration grid was used with a 6-31G**[38] [LANL2DZ[39] for Cr] basis set for geometry optimizations in Gaussian 09.[40] Vibrational frequency

analysis was performed to verify stationary points as either minima or first-order saddle points and to obtain standard enthalpy and Gibbs energy corrections (1 atm at 298 K) to the SCF energy. While we generally performed manual conformational searching we also used CREST[41] and xTB[42] for conformational searching of key transition states and intermediates that were likely to control 1-hexene purity (e.g. **TS3** and **TS11**). We also performed unrestricted M06-L/def2-TZVP[43,44,45,46] single point energies with the SMD[47] cyclohexane solvent and reported energies correspond to UM06-L/def2-TZVP//UM06-L/6-31G**[LANL2DZ for Cr]. Temperature and pressure corrected Gibbs energies as well as entropy-corrected Gibbs energies can be found in the Supporting Information (SI). These alternative Gibbs energies do not significantly change the relative energies in selectivity evaluation. We did not include an anionic counterion since Britovsek previously showed that counterion coordination in the second coordination sphere does not greatly impact the overall energies of the barriers.[48]

Energy landscapes for 1-hexene catalytic cycle and other C_6 catalytic cycles. We began by examining the 1-hexene catalytic cycle and alternative C_6 product forming pathways emanating from this cycle for catalyst **1a**. All structures examined for catalyst **1a** were also examined for catalysts **1c** and **2a**. In each case, the complete ligand was modeled without simplification. In our previous work we have demonstrated the necessity for including the entire ligand without modification.[49] All structures presented correspond to overall cationic Cr(III) complexes with a quartet spin state. We initially assumed that the most competitive alternative C_6 pathway would involve the blue catalytic cycle displayed in Scheme 2 that involves intermediates **F**, **G**, and **H**. Scheme 4 shows the relative Gibbs energies and enthalpies for the 1-hexene transition state, **TS3**, and the methylenecyclopentane up to the (cyclopentylmethyl)Cr(H) intermediate **G**. The *β*-

8

hydrogen transfer structure **TS3** is nearly 4 kcal/mol lower than the *β*-hydrogen elimination structure **TS5**, and this could suggest high selectivity for catalyst **1a**. However, the energy difference between **TS3** and **TS5** does not control 1-hexene purity. This is because the resulting Cr-H intermediate **F** is endergonic by 16.2 kcal/mol and the subsequent migratory insertion structure **TS6** requires 28.8 kcal/mol. While the energy difference between **TS6** and **TS3** could provide a model for 1-hexene purity, we thought that this energy difference was too large to be attenuated to be within a few kcal/mol for other catalysts with lower selectivity, such as catalyst **1c**. Indeed, for catalyst **1c**, the Gibbs barrier for **TS3** is 9.4 kcal/mol and the Gibbs barriers for **TS5** and **TS6** are 14.8 and 16.2 kcal/mol, respectively. For catalyst **1c**, while the barrier for **TS6** is lowered, the difference between **TS3** and **TS6** of 6.8 kcal/mol (~10^5 selectivity) is too large to be quantitatively or qualitatively compatible with the <50% 1-hexene selectivity found for this catalyst.
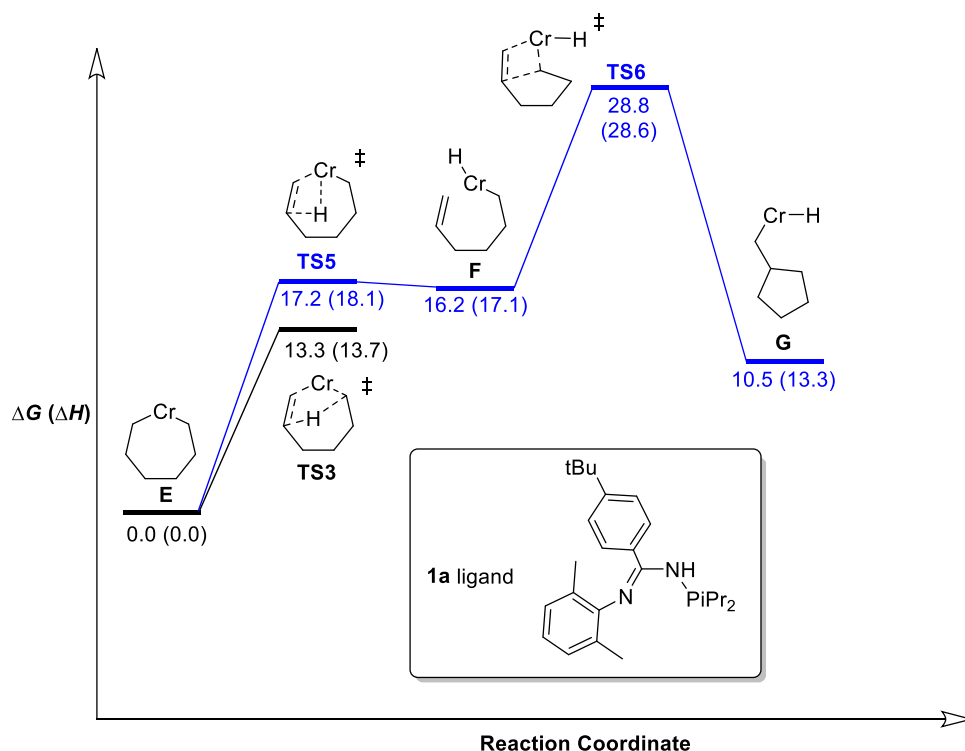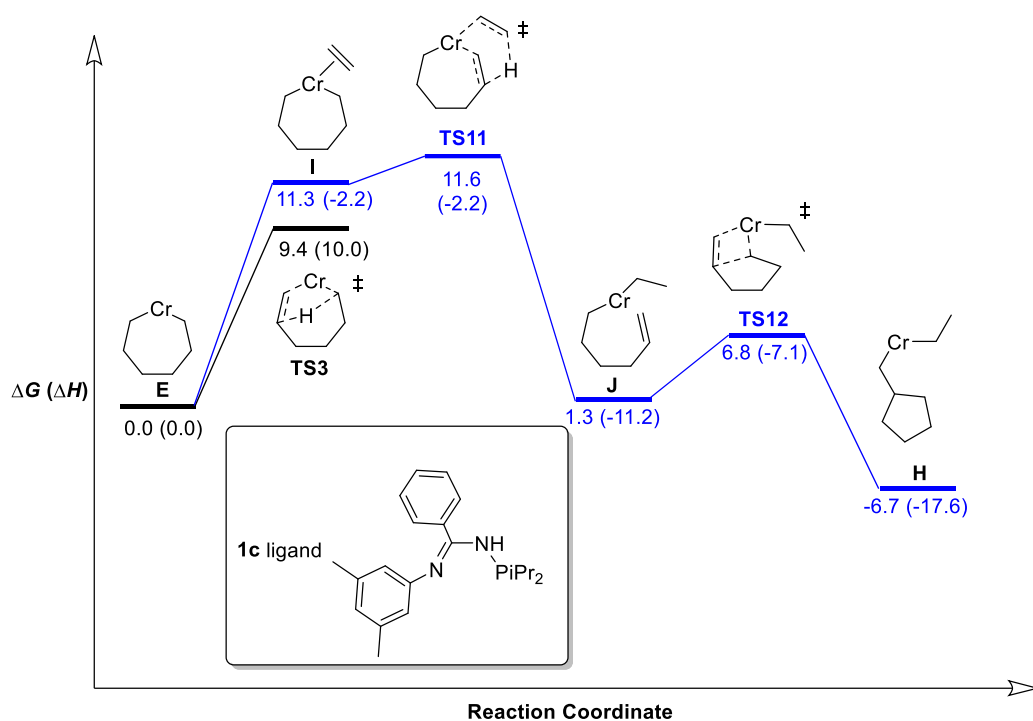
Scheme 4. Abbreviated Gibbs and enthalpy energy landscapes for catalyst **1c** starting from intermediate **E** and leading to 1-hexene (black) and methylenecyclopentane (blue). Energies in kcal/mol.

Because neither the energy difference between **TS3** and **TS5** or **TS6** likely control 1-hexene purity, we examined several alternative reaction pathways, many of which are outlined in Scheme 3. There are several pathways that are very high in energy and not competitive. For example, direct reductive elimination from **E** to give cyclohexane requires >40 kcal/mol, which is consistent with no cyclohexane C_6 product observed experimentally and previous calculations for bisphosphine Cr catalysts.[11,14,15] Because the energy of **TS6** is large, we examined C_6 pathways that circumvent this transition state. Of all the 1-hexene producing pathways we examined, the lowest energy pathway calculated was through ethylene coordination to **E** to give intermediate **I** followed by β-hydrogen transfer and migratory insertion to give **H**. Scheme 5 shows the energy

10

landscape for this pathway versus the 1-hexene transition state **TS3**. Coordination of ethylene to **E** is endergonic. The following β-hydrogen transfer **TS11** that leads to the Cr(ethyl) intermediate **J** requires a small barrier of <1 kcal/mol. Importantly, because barriers emanating from **J** are smaller than the reverse barrier from **J** to **TS11** there is no possibility for reversibility from this intermediate and therefore selectivity between 1-hexene and methylenecyclopentane is determined by the energy difference between **TS3** and **TS11**. Use of an energy span-type analysis confirms that **TS3** and **TS11** control selectivity when comparing these reaction pathways.[50,51,52]

Consistent with this lowest energy pathway for the (P,N)Cr catalyst **1a**, Britovsek and McGuuinness previously outlined this pathway as the lowest energy for bisphosphine Cr catalysts.[11,14,15] They found that β-hydride elimination from the metallacycloheptane followed by re-insertion and reductive elimination has a nearly 6 kcal/mol higher barrier than the pathway for 1-hexene and instead the most competitive pathway for non-1-hexene cyclic C_6 products involves β-hydrogen transfer to ethylene giving the Cr(ethyl)(hexenyl) complex and then re-insertion provides a pathway to the Cr(methylenecyclopentyl)(ethyl) complex.[11,14,15]

Scheme 5. Gibbs and enthalpy energy landscape starting from intermediate **E** and leading to 1-hexene (black) and methylenecyclopentane (blue). Energies in kcal/mol.

Consistent with the possibility that the energy difference between **TS3** and **TS11** controls 1-hexene purity, the pathway outlined in Scheme 5 also gives 1-octene, and several previous studies have correlated 1-octene production with the formation of cyclic C_6 products.[53] For example, Rosen and Klosin reported the purity of ethylene trimerization and tetramerization for several Cr bis(pholane) motif catalysts as well as other bisphosphines.[53] In this study, they found a strong correlation between 1-octene and cyclic product formation and the range of cyclic byproduct ratios formed by different catalysts, and this was proposed to support a mechanism that involves the common chromacycloheptane intermediate. For the pathways shown in Scheme 5, for catalyst **1c**, the $\Delta\Delta G^{\ddagger}$ (**TS11**-**TS3**) is 2.2 kcal/mol, which is consistent with substantial non-1-hexene C_6 products formed during catalysis. For catalyst **1a**, the $\Delta\Delta G^{\ddagger}$ between **TS11**-**TS3** is 7.6 kcal/mol, consistent with the extremely high selectivity found experimentally. Boltzmann

averaging of transition-state conformation energies did not significantly change the predicted selectivity between **TS11**-**TS3** for catalysts **1a** and **1c** (see SI).

We then calculated the $\Delta\Delta G^{\ddagger}$ between **TS11**-**TS3** for catalysts **1b**, **2a**, **2b**, and **2c** to determine if this energy difference can provide a general model for 1-hexene purity selectivity for (P,N)Cr catalysts. Indeed, the calculated values for these calculations are qualitatively consistent with experiment. For example, a $\Delta\Delta G^{\ddagger}$ of 2.5 kcal/mol for **1b**, while not as large as the energy difference for **1a**, is consistent with the >90% selectivity found experimentally. Similarly, for catalyst **2b** the calculated energy difference of 4.1 kcal/mol is consistent with the 97% selectivity found experimentally and the 0.4 kcal/mol energy difference for catalyst **2c** is also very similar with the 70% selectivity reported experimentally. The only significant discrepancy between calculated values and experimental selectivity was for catalyst **2a** where the calculated difference is 0.4, but **TS11** is lower than **TS3**. However, the energies of these transition states are close, and overall, there is a general qualitative correlation between the calculated selectivity and the experimental selectivity. Plotted in Figure 1 are $\Delta\Delta G^{\ddagger}$ values versus the natural log of the experimental ratio of 1-hexene versus all other C_6 mass products. The R^2 value of 0.5 is overall only semi-quantitative but suggests this is a viable model to predict high versus low 1-hexene purity.
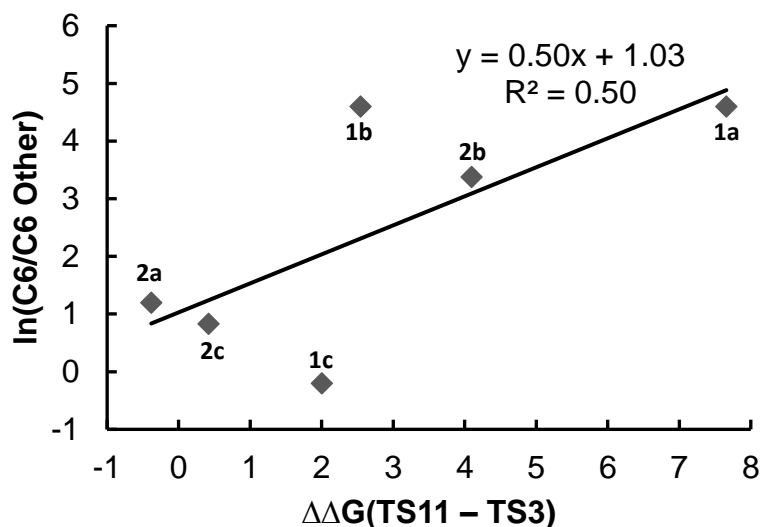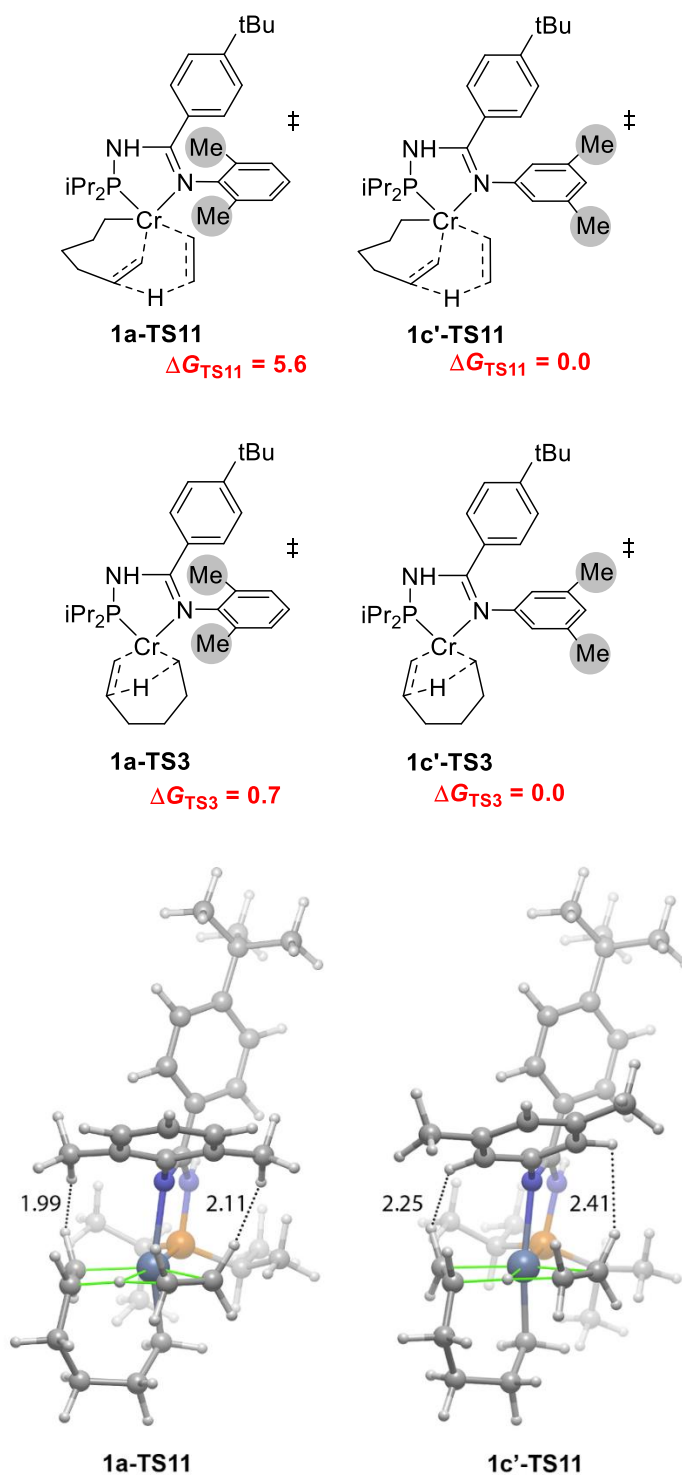
Catalyst	ln(C6/C6 other)	$\Delta\Delta G^{\ddagger}$
1a	4.6	7.7
1b	4.6	2.5
1c	-0.2	2.2
2a	1.2	-0.4
2b	3.4	4.1
2c	0.8	0.5

Figure 1. Plot of $\Delta\Delta G^{\ddagger}$ values versus the ln(1-hexene/all other C_6 mass products) for catalysts **1a**-**1c** and **2a**-**2c**.

Comparison of transition-state structures to understand relative 1-hexene purity for catalysts 1a and 1c. Because our DFT calculations accurately modeled the relative 1-hexene purity selectivity for catalysts **1a** and **1c** we wanted to understand the origin of selectivity. There are only two major differences between the ligands of catalysts **1a** and **1c**. For **1a**, the imine-substituted aryl group has 2,6-dimethyl groups while for **1c** the aryl group has 3,5-dimethyl groups. The second difference is that in **1a** there is a tBu-substituted aryl group while in **1c** this motif is a phenyl group. Because this ligand backbone aryl group is far away from the Cr metal center we decided

to analyze ligand **1a** versus **1c'** where this latter ligand has the tBu group added to ligand **1c**. This now makes it possible to directly compare transition state energies between catalysts.

Figure 2 gives the relative energies of the selectivity controlling transition-state structures **TS11** and **TS3** for catalysts **1a** and **1c'**. The energy difference between **TS3** is small with a value of only 0.7 kcal/mol. In contrast, the energy difference for **TS11** is 5.6 kcal/mol. This indicates that the large selectivity for catalyst **1a** and the low selectivity for catalyst **1c** is controlled by changes in **TS11** rather than significant energy changes in **TS3**. Importantly, this is consistent with both catalysts remaining highly active for forming 1-hexene through **TS3**. In-depth structure analysis (see the 3D structures in Figure 2) revealed that in **TS11** for catalyst **1a** the methyl groups from the imine aryl motif sterically encroach on the β-hydrogen transfer process. Specifically, one of the methyl groups repulses the side of the chromaheptacycle ring and the other methyl group sterically repulses the coordinated ethylene. The shortest distance between the hydrogen of the methyl group and the hydrogen of a methylene group of the chromacycle ring is 1.99 Å. A similar short distance also occurs between the other methyl group and the hydrogens of the coordinated ethylene (2.11 Å, see Figure 2). In contrast, both of these repulsive interactions are significantly relieved when the methyl groups are in the 3,5-positions. A similar structural analysis of **TS3** showed the distances between the imine-aryl methyl groups are much larger and less sterically repulsive.

1a-TS11
$\Delta G_{TS11} = 5.6$

1c'-TS11
$\Delta G_{TS11} = 0.0$

1a-TS3
$\Delta G_{TS3} = 0.7$

1c'-TS3
$\Delta G_{TS3} = 0.0$

1.99   2.11

2.25   2.41

1a-TS11

1c'-TS11

Figure 2. Top: Transition states and relative energies comparing catalysts **1a** and **1c'** for **TS11** and **TS3**. Relative energies reported in kcal/mol. Bottom: 3D representations of **TS11** for catalyst **1a** and **1c'** highlighting steric interactions with dotted lines. Green lines represent transition state partial bonds.

16

There have been other steric effects reported or proposed to influence catalytic Cr ethylene trimerization.[54] Experimentally, Makume examined purity for ethylene tetramerization with bisphosphine Cr catalysts where the steric bulk on the N-position of the ligand backbone partially controls purity.[55] As one recent example from a computational perspective, Liu and Liu used DFT calculations to understand trimerization/tetramerization selectivity for (2,2-dipicolylamine)Cr catalysts,[56,57] and in addition to the Cr charge controlling selectivity it was proposed that steric effects impact 1-hexene selectivity.

Conclusion

For several (P,N)Cr catalysts, M06-L DFT calculations were used to determine transition states and intermediates along the reaction pathways to 1-hexene and alternative C_6 mass products. This provided transition states with qualitative and semi-quantitative replication of the experimental 1-hexene purity values for six catalysts. While only semi-quantitative replication of experimental values was obtained, more important is that a clear selectivity controlling model has emerged. By directly comparing catalysts **1a** with the modified catalyst **1c'**, we were able to directly evaluate how impactful each transition state is on controlling 1-hexene purity. This analysis revealed that the key 1-hexene purity-controlling transition state is β-hydrogen transfer structures from the metallacycloheptane intermediate, and ligand steric interactions can significantly alter this transition state energy with a higher energy transition state leading to less alterative C_6 mass products. This work, in combination with the previous work by Britovsek and McGuuinness,[11,14,15] establishes a general set of transition states that can be used to analyze C_6

mass purity for future computational screening of new 1-hexene catalysts, because purity along with reactivity and catalyst lifetime are critical factors for new catalyst designs.

Corresponding Author

*dhe@chem.byu.edu and bischs@cpchem.com.

Author Contributions

All authors have given approval to the final version of the manuscript.

Conflict of Interest Statement

A patent application has been filed for subject matter contained in this article.

Supporting Information Available

Computational details, additional mechanisms, pressure and temperature corrections, and entropy-scaled energies.

References

1. Green, M. M.; Wittcoff, H. A., *Organic Chemistry Principles and Industrial Practice*, Wiley-VCH Verlag GmbH & Co. 2003; pp 1–22.

2. Weissermel, K.; Arpe, H.-J., *Industrial Organic Chemistry*. Chapter 3, 5th ed; Wiley-VCH Verlag GmbH & Co. 2010; 59–90.

3. Dixon, J. T.; Green, M. J.; Hess, F. M.; Morgan, D. H. Advances in selective ethylene trimerisation – a critical overview. *J. Organomet. Chem.* **2004**, *689*, 3641–3668.

4. McGuinness, D. S. Olefin Oligomerization via Metallacycles: Dimerization, Trimerization, Tetramerization, and Beyond. *Chem. Rev.* **2011**, *111*, 2321–2341.

5. Agapie, T. Selective ethylene oligomerization: Recent advances in chromium catalysis and mechanistic investigations. *Coord. Chem. Rev.* **2011**, *255*, 861–880.

6. Alferov, K. A.; Belov, G. P.; Meng, Y. Chromium catalysts for selective ethylene oligomerization to 1-hexene and 1-octene: Recent results. *Appl. Catal., A* **2017**, *542*, 71–124.

7. Kwon, D-H.; Maley, S. M.; Stanley, J. C.; Sydora, O. L.; Bischof, S. M.; Ess, D. H. Why Less Coordination Provides Higher Reactivity Chromium Phosphinoamidine Ethylene Trimerization Catalysts. *ACS Catal.* **2020**, *10*, 9674–9683.

8. Kwon, D.-H.; Fuller, J. T.; Kilgore, U. J.; Sydora, O. L.; Bischof, S. M.; Ess, D. H. Computational Transition-State Design Provides Experimentally Verified Cr(P,N) Catalysts for Control of Ethylene Trimerization and Tetramerization. *ACS Catal.* **2018**, *8*, 1138–1142.

9. Sydora, O. L.; Jones, T. C.; Small, B. L.; Nett, A. J.; Fischer, A. A.; Carney, M. J. Selective Ethylene Tri-/Tetramerization Catalysts. *ACS Catal.* **2012**, *2*, 2452–2455.

10. Kilgore, U. J.; Bischof, S. M.; Sydora, O. L. Catalyst Systems and Ethylene Oligomerization Method. US 10,196,328, 02/05/2019.

11. Britovsek, G. J. P.; McGuinness, D. S.; Wierenga, T. S.; Young, C. T. Single- and Double-Coordination Mechanism in Ethylene Tri- and Tetramerization with Cr/PNP Catalysts. *ACS Catal.* **2015**, *5*, 4152–4166.

12. Manyik, R. M.; Walker, W. E.; Wilson, T. P. A soluble chromium-based catalyst for ethylene trimerization and polymerization. *J. Catal.* **1977**, *47*, 197–209.

13. Emrich, R.; Heinemann, O.; Jolly, P. W.; Krüger, C.; Verhovnik, G. P. J. The Role of Metallacycles in the Chromium-Catalyzed Trimerization of Ethylene. *Organometallics* **1997**, *16*, 1511–1513.

14. Britovsek, G. J. P.; McGuinness, D. S. A DFT Mechanistic Study on Ethylene Tri- and Tetramerization with Cr/PNP Catalysts: Single versus Double Insertion Pathways. *Chem. Eur. J.* **2016**, *22*, 16891–16896.

15. Britovsek, G. J. P.; McGuinness, D. S.; Tomov, A. K. Mechanistic study of ethylene tri- and tetramerisation with Cr/PNP catalysts: effects of additional donors. *Catal. Sci. Technol.* **2016**, *6*, 8234–8241.

16. Hossain, M. A.; Kim, H. S.; Houk, K. N. Cheong, M. Spin-crossover in chromium-catalyzed ethylene trimerization: Density functional theory study. *Bull. Korean Chem. Soc.* **2014**, *35*, 2835–2838.

17. Yang, Y.; Liu, Z.; Zhong, L.; Qiu, P.; Dong, Q.; Cheng, R.; Vanderbilt, J.; Liu, B. Spin Surface Crossing between Chromium(I)/Sextet and Chromium(III)/Quartet without Deprotonation in SNS-Cr Mediated Ethylene Trimerization. *Organometallics* **2011,** *30*, 5297–5302.

18. Alam, F.; Zhang, L.; Zhai, Y.; Wanga, J.; Tang, H.; Chen, Y.; Jiang, T. In situ formed Cr(III) based silicon-bridged PNS systems for selective ethylene tri-/tetramerization. *J. Catal.* **2019**, *378*, 312–319.

19. Zhang, L.; Wei, W.; Alam, F.; Chena, Y.; Jiang, T. Efficient chromium-based catalysts for ethylene tri-/tetramerization switched by silicon-bridged/N,P-based ancillary ligands: a structural, catalytic and DFT study. *Catal. Sci. Technol.* **2017**, *7*, 5011−5018.

20. Alam, F.; Zhang, L.; Wei, W.; Wang, J.; Chen, Y.; Chunhua Dong, C.; Tao Jiang, T. Catalytic Systems Based on Chromium(III) Silylated-Diphosphinoamines for Selective Ethylene Tri-/Tetramerization. *ACS Catal.* **2018**, *8*, 10836−10845.

21. Zhang, L.; Meng, X.; Chen, Y.; Cao, C.; Jiang, T. Chromium-Based Ethylene Tetramerization Catalysts Supported by Silicon-Bridged Diphosphine Ligands: Further Combination of High Activity and Selectivity. *ChemCatChem* **2017**, *9*, 76−79.

22. Klemps, C.; Payet, E.; Magna, L.; Saussine, L.; Le Goff, X. F.; Le Floch, P. PCNCP Ligands in the Chromium-Catalyzed Oligomerization of Ethylene: Tri- versus Tetramerization. *Chem. Eur. J.* **2009**, *15*, 8259−8268.

23. Liu, L.; Liu, Z.; Cheng, R.; He, X.; Liu B. Unraveling the Effects of H_2, N Substituents and Secondary Ligands on Cr/PNP-Catalyzed Ethylene Selective Oligomerization. *Organometallics* **2018**, *37*, 3893−3900.

24. Yin, F.; Zhu, T.; Dong, C.; Li, B.; Zhang, L. H_2 promoting effect in Cr/PNP-catalyzed ethylene tetramerization: A density functional theory study. *Int. J. Quantum Chem.* **2021**, 121:e26667.

25. Albahily, K.; Fomitcheva, V.; Gambarotta, S.; Korobkov, I.; Murugesu, M.; Gorelsky, S. I. Preparation and Characterization of a Reduced Chromium Complex via Vinyl Oxidative Coupling:

Formation of a Self-Activating Catalyst for Selective Ethylene Trimerization. *J. Am. Chem. Soc.* **2011**, *133*, 6380–6387.

26. Bowen, L. E.; Haddow, M. F.; Orpen, A. G.; Wass, D. F. One electron oxidation of chromium N,N-bis(diarylphosphino)amine and bis(diarylphosphino)methane complexes relevant to ethene trimerisation and tetramerisation. *Dalton Trans.* **2007**, 1160–1168.

27. Rucklidge, A. J.; McGuinness, D. S.; Tooze, R. P.; Slawin, A. M. Z.; Pelletier, J. D. A.; Hanton, M. J.; Webb, P. B. Ethylene Tetramerization with Cationic Chromium(I) Complexes. *Organometallics* **2007**, *26*, 2782–2787.

28. Brückner, A.; Jabor, J. K.; McConnell, A. E. C.; Webb, P. B. Monitoring Structure and Valence State of Chromium Sites during Catalyst Formation and Ethylene Oligomerization by in Situ EPR Spectroscopy. *Organometallics* **2008**, *27*, 3849–3856.

29. Monillas, W. H.; Young, J. F.; Yap, G. P. A.; Theopold, K. H. A well-defined model system for the chromium-catalyzed selective oligomerization of ethylene. *Dalton Trans.* **2013**, *42*, 9198–9210.

30. Hirscher, N. A.; Labinger, J. A.; Agapie, T. Isotopic labelling in ethylene oligomerization: addressing the issue of 1-octene vs. 1-hexene selectivity. *Dalton Trans.* **2019**, *48*, 40–44.

31. Rosenthal, U. PNPN-H in Comparison to other PNP, PNPN and NPNPN Ligands for the Chromium Catalyzed Selective Ethylene Oligomerization. *ChemCatChem* **2020**, *12*, 41–52.

32. Agapie, T.; Schofer, S. J.; Labinger, J. A.; Bercaw, J. E. Mechanistic Studies of the Ethylene Trimerization Reaction with Chromium−Diphosphine Catalysts: Experimental Evidence for a Mechanism Involving Metallacyclic Intermediates. *J. Am. Chem. Soc.* **2004**, *126*, 1304–1305.

33. Agapie, T.; Labinger, J. A.; Bercaw, J. E. Mechanistic Studies of Olefin and Alkyne Trimerization with Chromium Catalysts: Deuterium Labeling and Studies of Regiochemistry Using a Model Chromacyclopentane Complex. *J. Am. Chem. Soc.* **2007**, *129*, 14281–14295.

34. Bhaduri, S.; Mukhopadhyay, S.; Kulkarni, S. A. Density functional studies on chromium catalyzed ethylene trimerization. *J. Organomet. Chem.* **2009**, *694*, 1297–1307.

35. Wang, Z.; Liu, L.; Ma, X.; Liu, Y.; Mi, P.; Liu, Z.; Zhang, J. Effect of an additional donor on decene formation in ethylene oligomerization catalyzed by a Cr/PCCP system: a combined experimental and DFT study. *Catal. Sci. Technol.* **2021**, *11*, 4596–4604.

36. Zhao, Y.; Truhlar, D. The M06 suite of density functionals for main group thermochemistry, thermochemical kinetics, noncovalent interactions, excited states, and transition elements: two new functionals and systematic testing of four M06-class functionals and 12 other functionals. *Theor. Chem. Acc.* **2008,** *120*, 215−241.

37. McGuinness, D. S.; Chan, B.; Britovsek, G. J. P.; Yates, B. F. Ethylene Trimerisation with Cr-PNP Catalysts: A Theoretical Benchmarking Study and Assessment of Catalyst Oxidation State. *Aust. J. Chem.* **2014**, *67*, 1481−1490.

38. Ditchfield, R.; Hehre, W. J.; Pople, J. A. Self-Consistent Molecular Orbital Methods. 9. Extended Gaussian-type basis for molecular-orbital studies of organic molecules. *J. Chem. Phys.* **1971**, *54*, 724.

39. Hay, P. J.; Wadt, W. R. Ab initio effective core potentials for molecular calculations. Potentials for the transition metal atoms Sc to Hg. *J. Chem. Phys.* **1985,** *82*, 270−283.

40. Gaussian 09, Revision B.01, M. J. Frisch, G. W. Trucks, H. B. Schlegel, G. E. Scuseria, M. A. Robb, J. R. Cheeseman, G. Scalmani, V. Barone, G. A. Petersson, H. Nakatsuji, X. Li, M. Caricato, A. Marenich, J. Bloino, B. G. Janesko, R. Gomperts, B. Mennucci, H. P. Hratchian, J.

V. Ortiz, A. F. Izmaylov, J. L. Sonnenberg, D. Williams-Young, F. Ding, F. Lipparini, F. Egidi, J. Goings, B. Peng, A. Petrone, T. Henderson, D. Ranasinghe, V. G. Zakrzewski, J. Gao, N. Rega, G. Zheng, W. Liang, M. Hada, M. Ehara, K. Toyota, R. Fukuda, J. Hasegawa, M. Ishida, T. Nakajima, Y. Honda, O. Kitao, H. Nakai, T. Vreven, K. Throssell, J. A. Montgomery, Jr., J. E. Peralta, F. Ogliaro, M. Bearpark, J. J. Heyd, E. Brothers, K. N. Kudin, V. N. Staroverov, T. Keith, R. Kobayashi, J. Normand, K. Raghavachari, A. Rendell, J. C. Burant, S. S. Iyengar, J. Tomasi, M. Cossi, J. M. Millam, M. Klene, C. Adamo, R. Cammi, J. W. Ochterski, R. L. Martin, K. Morokuma, O. Farkas, J. B. Foresman, and D. J. Fox, Gaussian, Inc., Wallingford CT, 2016.

41. Pracht, P.; Bohle, F.; Grimme, S. Automated exploration of the low-energy chemical space with fast quantum chemical methods. *Phys. Chem. Chem. Phys.* **2020**, *22*, 7169−7192.

42. Spicher, S.; Grimme, S. Robust Atomistic Modeling of Materials, Organometallic, and Biochemical Systems. *Angew. Chem. Int. Ed.* **2020**, *59*, 15665−15673.

43. Schäfer, A.; Horn, H.; Ahlrichs, R. Fully optimized contracted Gaussian basis sets for atoms Li to Kr. *J. Chem. Phys.* **1992**, *97*, 2571−2577.

44. Schäfer, A.; Huber, C.; Ahlrichs, R. Fully optimized contracted Gaussian-basis sets of triple zeta valence quality for atoms Li to Kr. *J. Chem. Phys.* **1994**, *100*, 5829−5835.

45. F. Weigend, F.; Ahlrichs, R. Balanced basis sets of split valence, triple zeta valence and quadruple zeta valence quality for H to Rn: Design and assessment of accuracy. *Phys. Chem. Chem. Phys.* **2005**, *7*, 3297−3305.

46. F. Weigend, F. Accurate Coulomb-fitting basis sets for H to Rn. *Phys. Chem. Chem. Phys.* **2006**, *8*, 1057−1065.

47. Marenich, A. V.; Cramer, C. J.; Truhlar, D. G. Universal Solvation Model Based on Solute Electron Density and on a Continuum Model of the Solvent Defined by the Bulk Dielectric Constant and Atomic Surface Tensions. *J. Phys. Chem. B* **2009**, *113*, 6378–6396.

48. Britovsek, G. J. P.; McGuinness, D. S.; Tomov, A. K. Mechanistic study of ethylene tri- and tetramerisation with Cr/PNP catalysts: effects of additional donors. *Catal. Sci. Technol.* **2016**, *6*, 8234−8241.

49. Kwon, D-H.; Small, B.; Sydroa, O. L.; Bischof, S. M.; Ess, D. H. The Challenge of Using Practical DFT to Model Fe Pendant Donor Diimine Catalyzed Ethylene Oligomerization. *J. Phys. Chem. B* **2019**, *123*, 3727−3739.

50. Kozuch, S.; Shaik, S. How to Conceptualize Catalytic Cycles? The Energetic Span Model. *Acc. Chem. Res.* **2011**, *44*, 101−110.

51. Uhe, A.; Kozuch, S.; Shaik, S. Automatic analysis of computed catalytic cycles. *J. Comput. Chem.* **2011**, *32*, 978−985.

52. Campbell, C. T. The Degree of Rate Control: A Powerful Tool for Catalysis Research. *ACS Catal.* **2017**, *7*, 2770−2779.

53. Boelter, S. D.; Davies, D. R.; Margl, P.; Milbrandt, K. A.; Mort, D.; Vanchura, B. A. II, Wilson, D. R.; Wiltzius, M.; Rosen, M. S.; Klosin, J. Phospholane-Based Ligands for Chromium-Catalyzed Ethylene Triand Tetramerization. *Organometallics* **2020**, *39*, 976−987.

54. Döhring, A.; Jensen, V. R.; Jolly, P. W.; Thiel, W.; Weber, J. C. Steric Control of the Chromium-Catalyzed Oligomerization of Ethylene. *Macromol. Symp.* **2001**, *173*, 117−121.

55. Makume, B. F.; Holzapfel, C. W.; Maumela, M. W.; J Willemse, J. A.; van den Berg, J. A. Ethylene Tetramerisation: A Structure-Selectivity Correlation. *ChemPlusChem* **2020**, *85*, 2308–2315.

56. Liu, L.; Liu, Z.; Tang, S.; Cheng, R.; He, X.; Liu, B. What Triggered the Switching from Ethylene-Selective Trimerization into Tetramerization over the Cr/(2,2′-Dipicolylamine) Catalysts? *ACS Catal.* **2019**, *9*, 10519−10527.

57. Gong, M.; Liu, Z.; Li, Y.; Ma, Y.; Sun, Q.; Zhang, J.; Liu B. Selective Co-Oligomerization of Ethylene and 1-Hexene by Chromium-PNP Catalysts: A DFT Study. *Organometallics* **2016**, *35*, 972−981.

TOC graphic